# An Empirical Study of Static Loading on Piezoelectric Stick-Slip Actuators of Micromanipulators

Aayush Damani, Manikantan Nambi, and Jake J. Abbott

**Abstract** Piezoelectric stick-slip actuators have become the foundation of modern micromanipulation. Due to difficulty in closed-loop control with manipulators that use piezoelectric stick-slip actuators, methods for open-loop control with a human in the loop have been developed. The utility of such methods depends directly on the accuracy of the open-loop models of the manipulator. Prior research has shown that modeling of piezoelectric actuators is not a trivial task as they are known to suffer from nonlinearities that degrade their performance. In this paper, we study the effect of static (non-inertial) loads on a prismatic and a rotary piezoelectric stick-slip actuator, and obtain a model relating the step size of the actuator to the load. The actuator-specific parameters of the model are calibrated by taking measurements in specific configurations of the manipulator. Results comparing the obtained model to experimental data are presented.

## 1 Introduction

Micromanipulation deals with small motions on the order of $10^{-3}$ to $10^{-6}$ m. Under the guidance of electron and optical microscopes, micromanipulation is now commonly used in the areas of MEMS construction and characterization, isolation and characterization of individual materials, and manipulation of single cells. The development and use of commercial manipulators like the Kleindiek MM3A [3], the Zyvex Nanomanipulator [5], Imina Technologies miBot [2], SmarAct Actuators [4], and the Attocube Nanopositioners [1] has increased with the demand for precise standardized tools for micromanipulation.

Piezoelectric stick-slip actuators have become the foundation of modern micromanipulation due to their simple structure, high positional accuracy, unlimited mov-

Aayush Damani, Manikantan Nambi, and Jake J. Abbott
Department of Mechanical Engineering, University of Utah, Salt Lake City, Utah, USA
e-mail: {aayush.damani,m.nambi,jake.abbott}@utah.edu

able distance, and high stability due to support by guiding surfaces [10]. Due to their useful characteristics, these actuators have been extensively used in manipulation of micro/nano-sized objects, medical devices, camera lens actuation systems, and in bio-sciences [7, 19]. These actuators consist of a piezoelectric element and a sliding mass that moves relative to the piezoelectric element (Fig. 1). Typically, these actuators have no sensor feedback (with the exception of SmarAct Actuators [4]), and hence, the individual joints of the manipulators are controlled open-loop, using one knob per joint. Due to difficulty in implementing real-time closed-loop controllers (which are generally based on vision feedback [9, 11]) for micromanipulators, methods to control them open-loop that capitalize on the intelligence of the human user are being developed [17, 20]. The utility of such methods depends directly on the accuracy of the open-loop models of the manipulator used.

Modeling of piezoelectric actuators is not a trivial task as they are known to suffer from nonlinearities such as hysteresis, creep, and drift, which degrade their performance [14, 12, 16]. A number of researchers have mathematically modeled the dynamics of piezoelectric stick-slip actuators [6, 8]. Peng *et al.* [18] used a presliding friction model to explain the dynamics of stick-slip actuators, and obtained an empirical model for the effect of end-effector mass on the step size of the actuator. Lockwood *et al.* [15] found that when gravitational force was acting parallel to the axis of their stick-slip actuator, the step size and corresponding displacement rate in the downward direction was observed to be 14.7% greater than in the upward direction. Thus, it is known that static (i.e., noninertial) loads in the direction of motion of the actuator increases the step size and vice-versa. However, this effect has not been well characterized in the past.

In this paper, we study the effect of static loads on a prismatic and a rotary piezoelectric stick-slip actuator, obtain an empirical model relating the step size to the load, and develop a method to calibrate the parameters of the empirical model using measurements from the actuators. The modeling experiments presented herein were performed for the coarse (stepping) mode of operation of the actuator (Fig. 1). The empirical models derived can be used with algorithms developed in [17] to perform intuitive teleoperation of the micromanipulator's end-effector, rather than

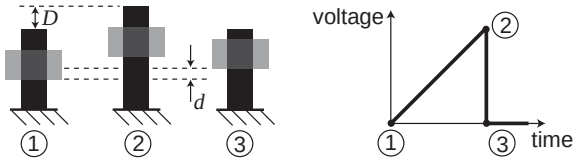


**Fig. 1** Functional description of a piezoelectric stick-slip actuator. A saw-tooth voltage is applied to the piezoelectric element. As the voltage slowly increases from 1 to 2, the piezoelectric element stretches by a distance $D$, and due to friction between the piezoelectric element and the sliding mass, the sliding mass also advances (stick phase). When the voltage is quickly reduced from 2 to 3, the piezoelectric element quickly shrinks, but the inertia of the sliding mass prohibits it from moving backward as quickly, resulting in a net forward displacement of the sliding mass of $d < D$ (slip phase). This is also known as the coarse mode of operation of the actuator. In the fine (traditional) mode, the voltage signal between 1 and 2 is controlled to achieve fine positioning.

controlling individual joints. With piezoelectric stick-slip actuators, the step size is stochastic, with a hard-to-model variance about a load-dependent mean. The method presented in this paper deals with modeling this mean. The method is primarily designed to provide an accurate estimate of the size of the next commanded step, such that a user's desired motion command can be accurately mapped to a required number of joint steps. Having a more accurate model of joint stepping could also lead to a method to estimate the joint configuration in manipulators without joint sensing, but such estimation methods would be subject to drift, and as such would need to incorporate additional sensing methods to be useful in practice.

## 2 Technical Approach

The commonly used Kleindiek MM3A manipulator is used in this study (Figs. 2 and 3). It has three degrees of freedom (DOF) with two rotary joints and one prismatic joint, which use piezoelectric stick-slip actuators. Due to the discrete step nature of these actuators, as well as the MM3A's controller, commands are given in the form of number of steps to be taken along a given joint. The joints of the MM3A lack sensor feedback, hence, it is difficult to obtain accurate measurements of the step size. To study the effect of static loads on the step size of a joint $j$, we use the average step size given by:

$$\overline{\gamma}_{ji} = \frac{R_j}{N_{ji}} \tag{1}$$

where $R_j$ is the total range of joint $j$ ($4\pi/3$ rad for the rotary joints and 12 mm for the prismatic joint), $N_{ji}$ is the total number of steps required by joint $j$ to travel through $R_j$, and $i \in \{+,-\}$ indicates the direction of joint motion.

As the step size for each joint is small (on the order of 1 $\mu$m), it is difficult to visually detect when a joint reaches its end of travel. However, the actuators make a distinct noise when they hit a mechanical stop. This knowledge is used to develop an audio limit switch that detects the end of travel for a joint. Custom software monitors the sound from a microphone at each instant and computes the Fast Fourier Transform (FFT) of the audio signal. The change in sound when a joint hits a mechanical stop is detected as a peak in the power of the FFT. The frequency at which this peak occurs, and the intensity of the peak, is different for each joint and has to be tuned before each experiment.

By measuring $\overline{\gamma}_{ji}$ at different configurations of the manipulator, we study the effect of gravitational loads on the rotary and the prismatic joint (no other external forces are acting on the manipulator). Because an individual joint cannot distinguish a gravitational load due to the distal links from an equivalent load due to a force applied at the end-effector (passing through the manipulator's Jacobian), our results generalize to all static (i.e., noninertial) loads. Nonlinear regression is used to fit a function, based on our knowledge of the load acting on the actuator, to the empirical data, to obtain a relation for the step size of the form $\gamma_{ji} = \Gamma_{ji}(g, \alpha_{ji})$, where $\alpha_{ji}$ is a set of actuator specific parameters, and $g$ is the gravity vector. The actuator specific

parameters $\alpha_{ji}$ of the model are then calibrated for by using $\overline{\gamma}_{ji}$ measurements at selected configurations for each joint. Significance of unmodeled factors such as change in environmental conditions from day to day are analyzed by performing ANOVA on the data obtained for $\overline{\gamma}_{ji}$.

## 3 Results

This section contains the main empirical modeling results of this paper. The experiments that were conducted to obtain these results are detailed in Section 4.

### *3.1 Effect of unmodeled factors*

Environmental conditions (e.g., temperature, humidity) are uncontrolled in our experiments, so we will not incorporate these factors into our model (although it is possible that they could be incorporated in the future [13]). To minimize these unmodeled effects on the open-loop control of the Kleindiek MM3A, we propose to calibrate the joints before each session of use. This assumes that there is a significant change from day to day that warrants such recalibration. To substantiate this claim, the average step size for prismatic joint 3 and the rotary joint 2 in the positive ($\overline{\gamma}_{3+}$ and $\overline{\gamma}_{2+}$) and negative ($\overline{\gamma}_{3-}$ and $\overline{\gamma}_{2-}$) directions were taken on two different days, which would incorporate a change in environmental conditions. The positive direction for the prismatic joint means moving out from 0 mm to 12 mm as defined by the $z_2$ direction. For the rotary joint, the positive direction is defined by the right-hand rule about the $z_1$ axis. For the prismatic joint, the configuration of the manipulator was kept constant at $q_2 = -\pi/2$, $\theta = 0$, and $\psi = 0$ on both days, and three readings each of the step size values $\overline{\gamma}_{3+}$ and $\overline{\gamma}_{3-}$ were taken on each day. For the rotary joint, $\overline{\gamma}_{2+}$ and $\overline{\gamma}_{2-}$ was recorded at $q_3$=0 mm, $\theta = -\pi/2$, and $\psi = 0$. In these configurations, there is no effect of gravity on the joint being investigated, isolating the unmodeled factors of interest.

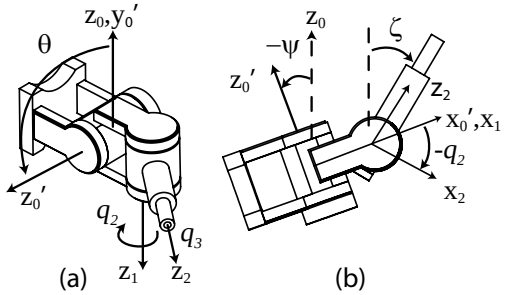


**Fig. 2** Kleindiek MM3A. With the $z_0$ axis initially vertical, the base frame is rotated by $\theta$ about $x_0$ and then rotated by $\psi$ about the new $y_0$. (a) Isometric view at $\theta = 90^\circ$. No gravitational loads acting on joints 2 or 3. (b) Side view at $\theta = 0^\circ$, with gravitational loads acting on both joints 2 and 3. $\zeta = \psi - q_2$.

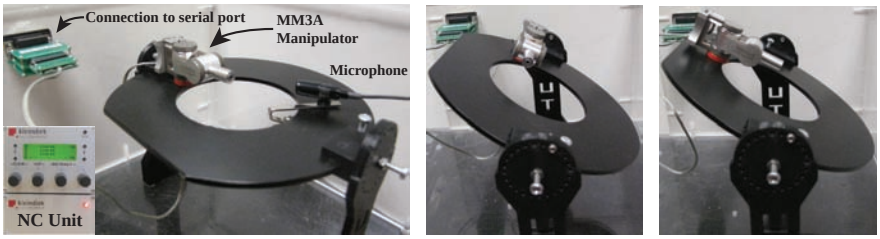


(a) (b) (c)

**Fig. 3** The Kleindiek MM3A manipulator is shown at different orientations. (a) $q_2 = -\pi/2$, $\theta = 0$, and $\psi = 0$; (b) $q_2 = -\pi/2$ and $\psi = 0$ at a particular $\theta$; (c) $q_2 = -\pi/2$ and $\theta = 0$ at a particular $\psi$.

An ANOVA test on the data shows that the difference in step size on different days is statistically significant ($p < 0.05$) for both positive and negative directions for both the prismatic and the rotary joints. The ANOVA test also shows a significant difference in the step size between the positive and negative directions within a given day for both joints. Thus, calibration is recommended each time the manipulator is to be used, and different calibration parameters should be found for each direction of motion.

## *3.2 Modeling of a prismatic joint*

Fig. 4 shows the results for the modeling experiments on the prismatic joint. The gravitational load on the prismatic joint is varied by changing the angles $q_2$, $\theta$, and $\psi$ (see Fig. 2). Curve 1 in Fig. 4a shows $\overline{\gamma}_{3+}$ recorded at $\theta = -\pi/2$ such that there is no load due to gravity along the joint regardless of $q_2$. At $q_2 = -\pi/2$ on curve 1, the entire structure of the manipulator is aligned with the axis of the prismatic joint, absorbing the recoil caused due to the quick stepping nature of the actuator, resulting in a maximum value for $\overline{\gamma}_{3+}$. The result from curve 1 is converted into an efficiency factor as:

$$\eta_i(q_2) = 1 - b_i|\cos q_2| \tag{2}$$

Joint 3 has a maximum stepping efficiency of 1 at $q_2 = -\pi/2$. The reduced step size (i.e., the reduction in stepping efficiency) at values of $q_2$ other than $-\pi/2$ is likely due to the component of the recoil force of the actuator acting perpendicular to the link connecting joint 1 to joint 2 causing a small deflection in the link (which is not infinitely rigid). This effect is captured by the $|\cos(q_2)|$ term in $\eta_i(q_2)$. The free parameter $b_i$ captures the loss of stepping efficiency when the prismatic joint is fully perpendicular to the maximum-efficiency configuration.

To isolate the effect of gravity without any loss of stepping efficiency due to recoil, $q_2$ is fixed at $-\pi/2$ such the manipulator arm is always outstretched, and the gravitational load is changed by varying $\psi$; results of this experiment are shown by curve 2, which is the pure effect of gravity on $\overline{\gamma}_{3+}$. Results for $\overline{\gamma}_{3-}$ are similar to

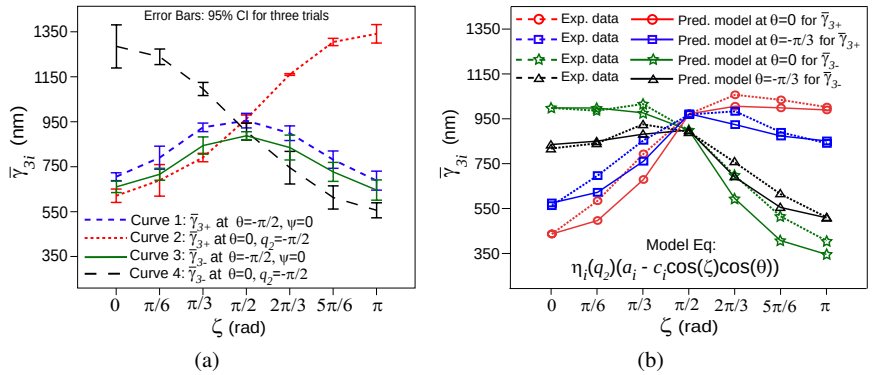


**Fig. 4** (a) Experimental data for the step size of the prismatic joint ($\overline{\gamma}_{3i}$) as a function of $\zeta$, plotted at $\theta = 0$ and $-\pi/2$, with data recorded on three different days. (b) Model equation fitted to experimental data for a single day (Day 1) at $\theta = 0$ and $-\pi/3$, with $\psi = 0$. Calibrated parameter values of $a_+ = 972$, $b_+ = 0.27$, $c_+ = 372$, $a_- = 899$, $b_- = 0.25$, and $c_- = -436$ were found using the three calibration configurations described in the text.

$\overline{\gamma}_{3+}$, but mirrored about $\zeta = \pi/2$ as can be been from curves 3 and 4 in Fig. 4a, indicating that moving joint 3 outward with $\zeta = 0$ is equivalent to moving joint 3 inward at $\zeta = \pi$.

We hypothesized a model that combines the information in curves 1 and 2 as:

$$\overline{\gamma}_{3i} = \eta_i(q_2)(a_i - c_i\cos(\zeta)\cos(\theta)) \tag{3}$$

The model has six actuator-dependent parameters ($\alpha_3 = \{a_+, a_-, b_+, b_-, c_+, c_-\}$) that can be identified by measuring $\overline{\gamma}_{3+}$ and $\overline{\gamma}_{3-}$ at the three different configurations: $(q_2, \theta, \psi) = (-\pi/2, 0, 0)$, $(0, -\pi/2, 0)$, and $(0, 0, 0)$. This process of finding the free parameters for the prismatic joint is explained in Section 3.3. The parameter $a_i$ represents the basic step size of the joint when no gravitational load or recoil inefficiency is acting on the joint, measured at $(-\pi/2, 0, 0)$. It can be seen that curve 1 and curve 2 intersect at the value of $a_i$. The term $c_i\cos(\zeta)\cos(\theta)$ is a function of the component of the gravitational load due to the weight of the distal link acting along the axis of the joint. The parameter $b_i$ was defined above.

### *3.3 Calibration procedure for a prismatic joint*

The step size model for the prismatic joint as described in Eq. 3 has six unknown parameters that can be calibrated for by taking six measurements of $\overline{\gamma}_{3i}$ as shown in Fig. 5. For simplicity, the average step size at a known configuration of $q_2$, $\theta$, and $\psi$ is denoted by $\overline{\gamma}_{3i(q_2,\theta,\psi)}$. The following procedure is used to identify the six free parameters $\alpha_3 = \{a_+, a_-, b_+, b_-, c_+, c_-\}$ of the prismatic joint:

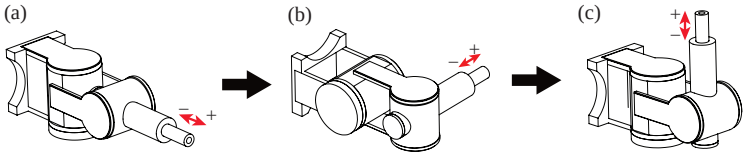


**Fig. 5** Calibrating configurations (in sequence) for identifying the six unknown parameters of the model of the prismatic joint (joint 3). (a) $a_i$ is calculated by measuring $\overline{\gamma}_{3i}$ at $(q_2, \theta, \psi)$ = (-$\pi$/2,0,0), (b) $b_i$ is calculated using $a_i$ calculated in the previous step and $\overline{\gamma}_{3i}$ at $(q_2, \theta, \psi)$= (0,-$\pi$/2,0), and (c) $c_i$ is calculated using the values of $a_i$ and $b_i$ above, and $\overline{\gamma}_{3i}$ at $(q_2, \theta, \psi)$= (0,0,0).

1. First, $\overline{\gamma}_{3+(-\pi/2,0,0)}$ and $\overline{\gamma}_{3-(-\pi/2,0,0)}$ are measured at $(q_2, \theta, \psi) = (-\pi/2, 0, 0)$ and by substituting in Eq. 3, we find parameter $a_i$ of the model by the following relation:

$$a_i = \overline{\gamma}_{3i(-\pi/2,0,0)} \tag{4}$$

2. Next, $\overline{\gamma}_{3+(0,-\pi/2,0)}$ and $\overline{\gamma}_{3-(0,-\pi/2,0)}$ are measured at $(q_2, \theta, \psi) = (0, -\pi/2, 0)$ and using Eq. 3 and the calculated value of $a_i$, we find parameter $b_i$ using the following relation:

$$b_i = 1 - \frac{\overline{\gamma}_{3i(0,-\pi/2,0)}}{a_i} \tag{5}$$

3. Finally, $\overline{\gamma}_{3+(0,0,0)}$ and $\overline{\gamma}_{3-(0,0,0)}$ are measured at $(q_2, \theta, \psi) = (0, 0, 0)$, and by substituting these values in Eq. 3 along with $a_i$ and $b_i$, we find parameter $c_i$ using the following relation:

$$c_i = a_i - \frac{\overline{\gamma}_{3i(0,0,0)}}{1 - b_i} \tag{6}$$

The order of the three steps above, which correspond to steps (a), (b), and (c), respectively, does not have to be carried out in any specific order. In practice, it may be more efficient to conduct the calibration in a different order that requires less joint movements (e.g., (b), (c), (a)).

Fig. 4b shows the model plotted against experimental data for a single day at $\theta = 0$ and $-\pi/3$ with $\psi$ fixed at 0. The value of $\theta = -\pi/3$ is not included as one of the calibration configurations mentioned above, yet the model captures the step size of the joint as a function of the configuration. We observe similar results in other configurations. Thus, the calibrated parameters can completely characterize the effect of the load due to gravity on the prismatic joint in any arbitrary configuration of the manipulator.

### *3.4 Modeling of a rotary joint*

Two experiments were performed to study the effect of gravitational loads on the rotary joint 2 (in an effort to study static loading in general). In experiment 1, $\theta$ is kept at $-\pi/2$ such that there is no load due to gravity on the joint, in an attempt to verify that the joint has a consistent behavior throughout its range of motion if other factors are controlled. Variation in $\overline{\gamma}_{2i}$ is studied in different sub-ranges of $q_2$, for $q_3 = 0$ mm and 12 mm. From the results of experiment 1, it is safe to conclude that the step size of the rotary joint is relatively constant throughout its range of motion when no load due to gravity is acting on the joint, since the variation in step size for different values of $q_2$ in this configuration is found to be less than $\pm 2\%$, with no discernible trend in the data. Fig. 6 shows the experimental results for experiment 2 in which $\theta$ is kept at zero such that there is load due to gravity on the joint; here the gravitational load on joint 2 is a function of its own position $q_2$.

The model for static loading on the rotary joint is derived based on the physics that, if $\theta = 0$, the torque on joint 2 is related to gravitational loads as $\tau_2 \propto g\sin(q_2)$, where $g$ is the acceleration due to gravity; the constant of proportionality is related to the mass and lengths of the distal links, which are unknown to us. The empirical model to predict the step size for the rotary joint is formulated as:

$$\gamma_{2i} = \gamma_{2i,\theta=\pm\pi/2} + d_i \sin(\zeta) \tag{7}$$

where $\gamma_{2i,\theta=\pm\pi/2}$ denotes the direction-dependent step size of the rotary joint when there is no effect of gravity on the link (i.e., at $\theta = \pm\pi/2$), $d_i$ is a free parameter that denotes the maximum increase in step size over the baseline step size $\gamma_{2i,\theta=\pm\pi/2}$, and $\zeta = \psi - q_2$ as described in Fig. 2. We assume that the step size at $\theta = -\pi/2$ and $\theta = \pi/2$ would be equal to the step size at $q_2 = 0$ and $q_2 = -\pi$ when $\psi = \theta = 0$, since there is no torque due to gravity on the joint in any of these cases.

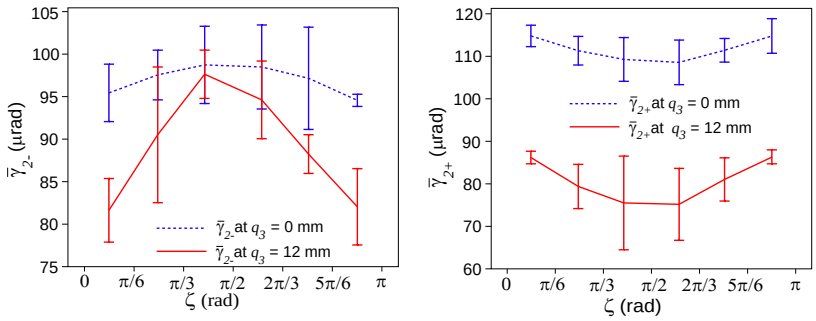


**Fig. 6** Step size (a) $\overline{\gamma}_{2-}$ and (b) $\overline{\gamma}_{2+}$ as a function of $\zeta$ at $q_3 = 0$ and 12 mm, $\psi = 0$, and $\theta = 0$. $\overline{\gamma}_{2i}$ is recorded for intervals of $\pi/6$ from $-\pi/6$ to $7\pi/6$ and is plotted at the midpoint of each interval as explained in Section 4.

It can be seen that the nature of step size in the positive direction is an inverted form of its nature in the negative direction. This is attributed to the fact that the load due to gravity acts against the direction of motion of the joint in the positive direction, and with it in the negative direction. Hence, the step size obtained in the positive direction, $\overline{\gamma}_{2+}$, will be less than that obtained at $\theta = -\pi/2$ where no gravitation load is acting on the joint. The opposite holds true for the step size in negative direction, $\overline{\gamma}_{2-}$. In other words, downward steps are bigger that horizontal steps, which in turn are bigger than upward steps, as we would expect.

If the manipulator were to be tilted by an angle $\theta \neq 0$, then the torque due to gravity on joint 2 would become proportional to the cosine of the gravitational component, such that the model of Eq. 7 should be modified as:

$$\gamma_{2i} = \gamma_{2i,\theta=\pm\pi/2} + d_i \sin(\zeta)\cos(\theta) \tag{8}$$

### *3.5 Calibration procedure for a rotary joint*

Fig. 7 shows the calibration sequence for rotary joint 2, which gives us values for the joint-specific parameters, $d_i$ and $\overline{\gamma}_{2i,\theta=\pm\pi/2}$, for the rotary joint in the positive and negative directions. For simplicity, the average step size at a known configuration of $q_3$, $\theta$, and $\psi$ is denoted by $\overline{\gamma}_{2(q_3,\theta,\psi)}$ unless otherwise mentioned. The following procedure is followed to obtain the free parameter:

1. $\overline{\gamma}_{2-(0,0,0)}$ and $\overline{\gamma}_{2+(0,0,0)}$ are measured by driving joint 2 across its range from $q_2 = \pi/6$ to $-7\pi/6$ in the negative direction and then in the positive direction at $(q_3, \theta, \psi) = (0,0,0)$.
2. The prismatic joint is then fully extended. $\overline{\gamma}_{2-(12,0,0)}$ and $\overline{\gamma}_{2+(12,0,0)}$ are measured by driving joint 2 across its range from $q_2 = \pi/6$ to $-7\pi/6$ in the negative direction and then in the positive direction at $(q_3, \theta, \psi) = (12\,\text{mm}, 0, 0)$.
3. The manipulator is then tilted by setting $\theta = -\pi/2$ such that there is no gravitational torque on joint 2. $\overline{\gamma}_{2-(12,-\pi/2,0)}$ and $\overline{\gamma}_{2+(12,-\pi/2,0)}$ are measured by driving joint 2 across its range from $q_2 = \pi/6$ to $-7\pi/6$ in the negative direction and then in the positive direction at $(q_3, \theta, \psi) = (12\,\text{mm}, -\pi/2, 0)$.
4. The prismatic joint is then fully retracted. $\overline{\gamma}_{2-(12,-\pi/2,0)}$ and $\overline{\gamma}_{2+(12,-\pi/2,0)}$ are measured by driving joint 2 across its range from $q_2 = \pi/6$ to $-7\pi/6$ in the negative direction and then in the positive direction at $(q_3, \theta, \psi) = (0\,\text{mm}, -\pi/2, 0)$.

Since $\gamma_2$ is a function of $q_2$ at each instant, it not a trivial task to calculate the parameter $d_i$ from Eq. 8 by using the average step size values ($\overline{\gamma}_{2i}$) that are available to us based on the entire range of motion. A simulation of the model shown in Eq. 8 was implemented wherein a number of different values of the free parameters $\overline{\gamma}_{2i,\theta=-\pi/2}$ and $d_i$ were given to the simulation as inputs, and the simulation returns the step size at each instant and the total number of steps required to move through the joint's entire range. The total number of steps obtained is then used to calculate the simulated average step size $\overline{\gamma}_{2i,\theta=0}$.

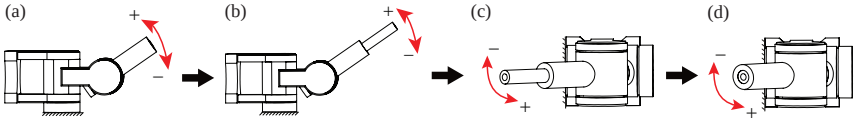


**Fig. 7** Calibrating configurations (in sequence) for identifying the six unknown parameters of the model of the rotary joint 2. $q_2$ is driven across its full range from $\pi/6$ to -$7\pi/6$ in the negative and positive directions at (a) $q_3 = 0$ mm, $\theta = 0$, and $\psi = 0$; (b) $q_3 = 12$ mm, $\theta = 0$, and $\psi = 0$; (c) $q_3 = 12$ mm, $\theta = -\pi/2$, and $\psi = 0$; and (d) $q_3 = 0$ mm, $\theta = -\pi/2$, and $\psi = 0$.

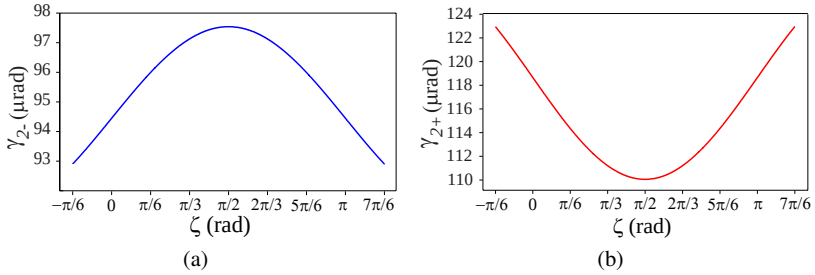


**Fig. 8** Simulated model of the step size of joint 2 in (a) the negative direction, and in (b) the positive direction. The values of $\overline{\gamma}_{2,\theta=0}$ and $\overline{\gamma}_{2,\theta=-\pi/2}$ are fixed, and $\theta$ was kept at zero in simulation. The nature of data obtained in simulation agrees with experimental results shown in Fig. 6.

Fig. 8 shows the simulation results obtained for the rotary joint after stepping $q_2$ through its full range of motion from $\pi/6$ to $-7\pi/6$ for fixed arbitrary (typical) values of $\overline{\gamma}_{2i,\theta=-\pi/2}$ and $d_i$. The figure shows the dependence of step size on the current configuration. This validates our model of the rotary joint 2 with data observed in experiments (Fig. 6). It was found that the difference between the two average step size values $\overline{\gamma}_{2i,\theta=0}$ and $\overline{\gamma}_{2i,\theta=-\pi/2}$ have a quadratic relation with the free parameter $d_i$ as shown in Fig. 9. Irrespective of the *individual* values of $\overline{\gamma}_{2i,\theta=0}$ and $\overline{\gamma}_{2i,\theta=-\pi/2}$, the free parameter value $d_i$ remains the same (difference of less than 1 $\mu$rad) for the same *difference* between the two step size values. The simulation was performed such that the range of values for $\overline{\gamma}_{2i,\theta=0} - \overline{\gamma}_{2i,\theta=-\pi/2}$ obtained in simulation was from $-9.2\,\mu$rad to $9.2\,\mu$rad, because this was the range of $\overline{\gamma}_{2i,\theta=0} - \overline{\gamma}_{2i,\theta=-\pi/2}$ observed in experiments. A relation for computing $d_i$ was formulated by fitting the simulation results obtained to a quadratic function as shown in Fig. 9. The equation formulated using nonlinear least-squares regression is:

$$d_i = 3.41(\overline{\gamma}_{2i,\theta=0} - \overline{\gamma}_{2i,\theta=-\pi/2})^2 + 0.025(\overline{\gamma}_{2i,\theta=0} - \overline{\gamma}_{2i,\theta=-\pi/2}) + 6.42 \times 10^{-7} \tag{9}$$

From Fig. 6, we see that $\overline{\gamma}_{2i,\theta=-\pi/2}$ and $d_i$ are a function of $q_3$, as $q_3$ changes the inertial load on joint 2. Different values of $d_i$ can be calculated when $q_3 = 0$

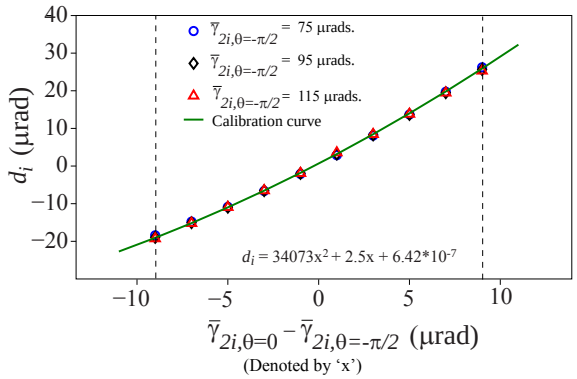


**Fig. 9** Variation of the free parameter $d_i$ with respect to change in difference between $\bar{\gamma}_{2i,\theta=0}$ and $\bar{\gamma}_{2i,\theta=-\pi/2}$ at different values of $\bar{\gamma}_{2i,\theta=-\pi/2}$. The vertical dash lines represent the range of this difference as observed in experiments.

and 12 mm using Eq. 9, and the effect of changing $q_3$ is reflected in the values of $\bar{\gamma}_{2i,\theta=0}$ and $\bar{\gamma}_{2i,\theta=-\pi/2}$. The relation between $d_i$ and $q_3$ cannot be derived with just two data points, and this change in step size due to inertial loading will be studied in the future, but we find a simple linear interpolation provides accurate results.

Fig. 10a-d shows the predicted model for $\gamma_{2i}$ after computing $d_i$ via calibration against experimental data collected on a single day with $q_3 = 0$ and 12 mm. Fig. 10e-f shows the data collected at $\theta = -\pi/4$ which is used to test the validity of the model for $\theta \neq 0$. The predicted models obtained after calibration are found to be accurate to within 1 $\mu$rad ($\pm 2\%$). Thus, the free parameters for the rotary joint can be calibrated for by using eight $\bar{\gamma}_{2i}$ measurements.

## 4 Experiments

The experiments in this paper were designed to isolate and study the effect of static loads on the rotary and prismatic joints of a Kleindiek MM3A. The gravitational load acting on the prismatic joint (joint 3) along the direction of its motion can be described by the angles $q_2$, $\theta$, and $\psi$ (Fig. 2). To study the effect of gravity on the prismatic joint, data was recorded in two different experiments. For each value of $q_2$, $\theta$, and $\psi$, $\bar{\gamma}_{3+}$ was first recorded followed by $\bar{\gamma}_{3-}$. In experiment 1, $\bar{\gamma}_{3+}$ and $\bar{\gamma}_{3-}$ were recorded at different values of $q_2$ and $\theta$ in the range of 0 to $\pi$ and 0 to $-\pi/2$, respectively, in increments of $\pi/6$ with $\psi$ fixed at 0. For each value of $q_2$, data was recorded for different values of $\theta$ before moving on to the next value of $q_2$. In experiment 2, $q_2$ was fixed at $-\pi/2$ (outstretched) and the gravitational load was varied by changing $\psi$, with $\theta = 0$. $\bar{\gamma}_{3+}$ and $\bar{\gamma}_{3-}$ were recorded for one condition in experiment 1 followed by the corresponding condition in experiment 2, before recording data for the next condition in both experiments. This distributes

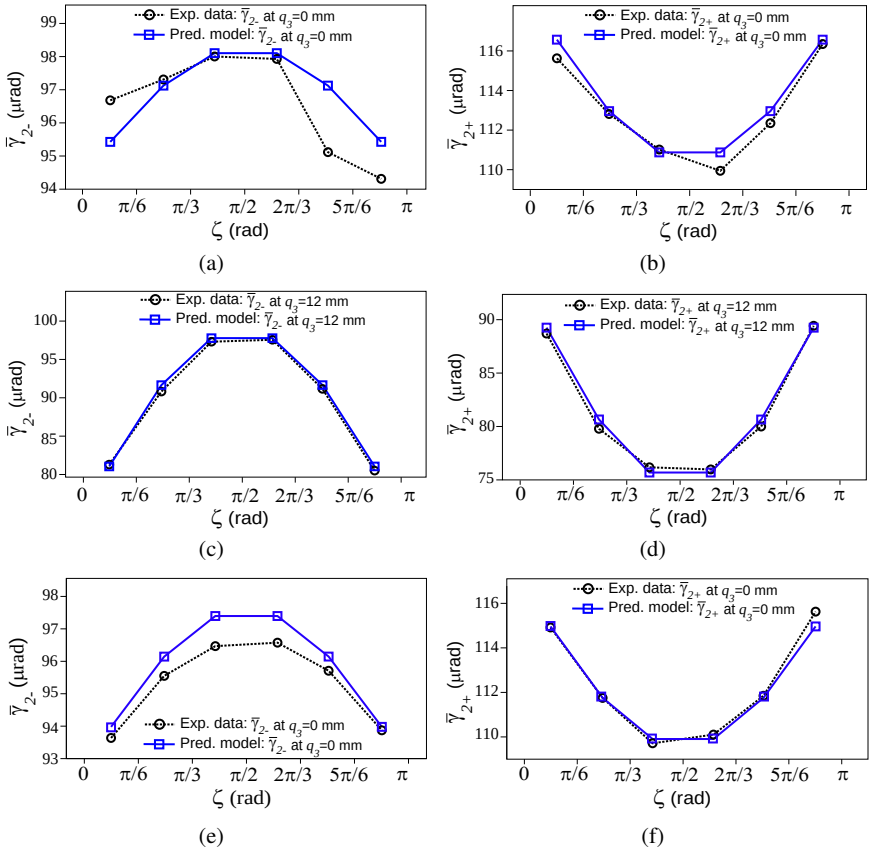


**Fig. 10** (a) Model equation fitted to experimental data taken on a single day for $\overline{\gamma}_{2i}$ at (a) $q_3 = 0$ mm, $\theta = 0$, $\psi = 0$ in the negative direction, with $d_-$=3.83 $\mu$rad (b) $q_3 = 0$ mm, $\theta = 0$, $\psi = 0$ the in positive direction, with $d_+$=-8.15 $\mu$rad (c) $q_3 = 12$ mm, $\theta = 0$, $\psi = 0$ in the negative direction, with $d_-$=23.94 $\mu$rad(d) $q_3 = 12$ mm, $\theta = 0$, $\psi = 0$ in the positive direction, with $d_+$=-19.40 $\mu$rad (e) $q_3 = 0$ mm, $\theta = -\pi/4$, $\psi = 0$ in the negative direction, with $d_-$=6.91 $\mu$rad (f) $q_3 = 0$ mm, $\theta = -\pi/4$, $\psi = 0$ in the positive direction, with $d_+$=-10.24 $\mu$rad.

any drift in $\overline{\gamma}_{3+}$ and $\overline{\gamma}_{3-}$ due to time equally in both experiments. One trial for each condition in both experiments was taken per day for three consecutive days to take into account the effect of unmodeled changes in environmental conditions. Curves 1 and 3 in Fig. 4a are obtained from $\overline{\gamma}_{3+}$ and $\overline{\gamma}_{3-}$, respectively, recorded in experiment 1 using the values when $\theta = -\pi/2$, for all three days. Curves 2 and 4 are obtained from $\overline{\gamma}_{3+}$ and $\overline{\gamma}_{3-}$, respectively, recorded in experiment 2. Fig. 4b shows $\overline{\gamma}_{3+}$ and $\overline{\gamma}_{3-}$for experiment 1 recorded on Day 1 when $\theta = 0$ and $-\pi/3$. Data from experiments 1 and 2 performed on the same day were used to derive the model parameters shown in Fig. 4b.

For modeling a rotary joint, two experiments were performed on joint 2. Initially, $\overline{\gamma}_{2+}$ and $\overline{\gamma}_{2-}$ was measured for the entire range of motion for the joint with $q_3 =$ 0 mm and 12 mm. Using a custom-made fixture, joint 2 was then moved in intervals of $\pi/6$ for $q_2$ from 0 to $\pi$ and $\overline{\gamma}_{2i}$ was calculated for each interval. The average step size of each interval is assumed to be the step size at the midpoint of the interval as shown in Fig. 6. This allows us to study the variation in $\overline{\gamma}_{2i}$ as a function of $q_2$. $\overline{\gamma}_{2i}$ was recorded in both negative ($\overline{\gamma}_{2-}$) and positive ($\overline{\gamma}_{2+}$) directions. In experiment 1, the mentioned sequence of collecting data was performed at $\theta = -\pi/2$. When $\theta = -\pi/2$, there is no torque due to gravity on the rotary joint, and the step size observed is purely due to the inertial load on the joint and the inherent properties of the actuator. In experiment 2, $\theta$ is kept at zero. A gravitational torque is present on the rotary joint, and the step size obtained is influenced by gravitational loading on the joint. One set of data for both experiments was recorded on three different days. Fig. 6 shows the results for $\overline{\gamma}_{2i}$ in experiment 2 for all three days, with $\theta = 0$. Fig. 10a-d shows the data for $\overline{\gamma}_{2i}$ from experiment 2 for a single day with the predicted model fitted to the experimental data. An additional set of data was recorded at $\theta = -\pi/4$ to check the validity of the model described in Eq. 8, the results of which are shown in Fig. 10e-f.

## 5 Main Experimental Insights

From the experiments performed in this paper, it was concluded that the step size of a piezoelectric stick-slip actuator can be modeled as having two summed components—a baseline step size that occurs when there is no static load acting on the joint, and a positive/negative contribution due to any static load acting on the joint—and that this two-component step size must be modified to account for the manipulator being in a configuration in which its compliance decreases the efficiency of the stick-slip movement.

Models relating the step size to the static loads were developed for a prismatic (joint 3) and a rotary joint (joint 2) of the Kleindiek MM3A. The actuator-specific parameters of the model can be calibrated for by taking 14 measurements of the average step size (6 for the prismatic joint and 8 for the rotary joint) in specific configurations of the manipulator. The models can accurately predict the step size of the joints at a given manipulator configuration. Kleindiek does not provide specifications for step size of the joints of the MM3A, so we compare the accuracy of our model to a simpler constant-step-size model when there is no static load acting on the joints, i.e., $\overline{\gamma}_{3i}$ at $(q_2, \theta, \psi)$=$(-\pi/2, 0, 0)$ for the prismatic joint, and $\overline{\gamma}_{2i}$ at $(q_3, \theta, \psi)$=(0,0,0) for the rotary joint. The maximum error in the developed model is approximately 15% for the prismatic joint, and 2% for the rotary joint, as compared to 40% and 7% for the prismatic and rotary joints, respectively, when using the constant-step-size model. Changes in environmental conditions have an effect on the parameters of the model; consequently, the model for the joint parameters should be recalibrated each day.

Fig. 6 shows that there is a significant effect of the joint 3 variable $q_3$ on the step size of the rotary joint 2. Also, $\overline{\gamma}_{2i,\theta=-\pi/2}$ and $d_i$ are functions of $q_3$. This is expected, as a change in $q_3$ will lead to a change in inertial load on joint 2 and a change in the step size of joint 2. The effect of inertial loads on the step size are not addressed herein and will be studied in the future.

Joint 1 is another rotary joint with the same range as joint 2 and having the same properties except for the change in static load value. Hence, the model and calibration routine for joint 2 can be extended to joint 1. The only difference in the calibration routine would be that at $\theta = 0$ there is no effect of gravity on joint 1, while at $\theta = -\pi/2$ the gravity is perpendicular to the joint axis. So, in short, the definition of the terms, $\overline{\gamma}_{2i,\theta=0}$ and $\overline{\gamma}_{2i,\theta=-\pi/2}$ would be interchanged.

Models developed in this paper for the step size of piezoelectric stick-slip actuators are not perfect. Hence, when these models are used in teleoperation algorithms like the one proposed in [17], there will be drift in the position of the end-effector due to the accumulation of error in the model. However, this problem can be overcome as recently developed piezoelectric actuators have sensors with micro- and nanometer resolution [4]. This sensor feedback could be used to remove drift in the position, but the models of step size will still be necessary to command multiple steps in a single command to the joint before sensor feedback is obtained.

The experiments in this paper were performed in a room without tight climate control. When using the manipulator inside an SEM, frequent recalibration might not be necessary, since the manipulator will be in a vacuum. However, the audio limit switch used to detect end of travel will not work in a vacuum, and will need to be replaced by an accelerometer-based sensor mounted on the manipulator (when sensor feedback is not available) to detect the end of travel during calibration.The experiments in this paper were performed using a Kliendiek MM3A, but we expect the results to generalize to other similar devices that utilize peizoelectric stick-slip actuators.

## References

1. Attocube Nanopositioners. http://www.attocube.com/
2. Imina Techonologies miBot. http://http://www.imina.ch/
3. Kleindiek Nanotechnik MM3A. http://www.nanotechnik.com/
4. SmarAct GmbH. http://www.smaract.de
5. Zyvex Nanomanipulator. http://www.zyvex.com/
6. Breguet, J.M., Clavel, R.: Stick and slip actuators: design, control, performances and applications. In: Proc. Micromechatronics and Human Science, pp. 89–95 (1998)
7. Breguet, J.M., Driesen, W., Kaegi, F., Cimprich, T.: Applications of piezo-actuated microrobots in micro-biology and material science. pp. 57–62 (2007)
8. Chang, S.H., Li, S.S.: A high resolution long travel friction-drive micropositioner with programmable step size. Review of Scientific Instruments **70**(6), 2776–2782 (1999)
9. Fatikow, S., Wich, T., Hülsen, H., Sievers, T., Jähnisch, M.: Microbot system for automatic nanohandling inside a scanning electron microscope. IEEE/ASME Trans. Mechatronics **12**(3), 244–252 (2007)

10. Higuchi, T., Yamagata, Y.: Micro robot arm utilizing rapid deformations of peizoelectric elements. Advanced Robotics **6**(3), 353–360 (1992)
11. Hötzendorfer, H., Giouroudi, I., Bou, S., Ferros, M.: Evaluation of different control algorithms for a micromanipulation system. In: Int. Conf. Engineering and Mathematics (2006)
12. Jung, H., Shim, J.Y., Gweon, D.: New open-loop actuating method of piezoelectric actuators for removing hysteresis and creep. Review of Scientific Instruments **71**(9), 3436–3440 (2000)
13. Li, J.W., Yang, G.S., Zhang, W.J., Tu, S.D., Chen, X.B.: Thermal effect on piezoelectric stick-slip actuator systems. Review of Scientific Instruments **79**(4), 046108 (2008)
14. Liaw, H.C., Shirinzadeh, B., Smith, J.: Enhanced sliding mode motion tracking control of piezoelectric actuators. Sensors and Actuators A: Physical **138**(1), 194–202 (2007)
15. Lockwood, A.J., Wang, J.J., Gay, R., Inkson, B.J.: Characterising performance of TEM compatible nanomanipulation slip-stick intertial sliders against gravity. Jounal of Physics:Conference Series **126**(1) (2008)
16. Lv, Y., Wei, Y.: Study on open-loop precision positioning control of a micropositioning platform using a piezoelectric actuator. In: Proc. World Congress on Intelligent Control and Automation, pp. 1255–1259 (2004)
17. Nambi, M., Damani, A., Abbott, J.J.: Toward intuitive teleoperation of micro/nanomanipulators with piezoelectric stick-slip actuators. In: Proc. IEEE/RSJ Int. Conf. Intelligent Robots and Systems, pp. 445–450 (2011)
18. Peng, J.Y., Chen, X.B.: Modeling of piezoelectric-driven stick-slip actuators. IEEE/ASME Trans. Mechatronics **16**(2), 394–399 (2011)
19. Schurzig, D., Labadie, R.F., Hussong, A., Rau, T.S., Webster III, R.J.: Design of a tool integrating force sensing with automated insertion in cochlear implantation. IEEE/ASEM Trans. Mechatronics **17**(2), 381–389 (2012)
20. Tonet, O., Marinelli, M., Megali, G., Sieber, A., Valdastri, P., Menciassi, A., Dario, P.: Control of a teleoperated nanomanipulator with time delay under direct vision feedback. In: Proc. IEEE Int. Conf. Robotics and Automation, pp. 3514–3519 (2007)